Investigation of Hybrid Grid-Based CFD Methods for Rotorcraft Flow Analysis

Glen R. Whitehouse
glen@continuum-dynamics.com
Continuum Dynamics, Inc.
Ewing, New Jersey, 08618

and

Hormoz Tadghighi
hormoz.tadghighi@boeing.com
Boeing Company
Mesa, AZ

Abstract

Accurate flow prediction is essential to the design and development of rotorcraft, and whilst current numerical analysis tools can, in principle, model the complete flow field, in practice the accuracy of these tools is hampered by various inherent numerical deficiencies. For example, Lagrangian vortex filament methods lose accuracy when the rotor wake undergoes large distortions since the detailed dynamics of vortical structures within the wake must then be modeled empirically. Grid-based CFD methods, on the other hand, introduce non-physical dissipation that can quickly smear regions of vorticity leading to poor performance predictions. Recently, it has been shown that numerical diffusion of the rotor wake can be controlled in a grid based solver, based on a vorticity-velocity rather than pressure-velocity formulation, by carefully constructing the flux formula and selecting an appropriate flux limiter. Using such techniques, a CFD module, VorTran-M, has been developed that solves the vorticity-velocity formulation of the Navier-Stokes equations, and can be coupled, using pseudo overset methods, to conventional pressure-velocity based CFD methods to simulate vorticity dominated flows. This paper describes ongoing work coupling VorTran-M to the OVERFLOW overset grid RANS solver. After a brief description of the module, coupling strategies and prior coupling work, preliminary results obtained with the coupled OVERFLOW/VorTran-M are presented.

Nomenclature

C_T	thrust coefficient, $T/\rho\pi R^2(\Omega R)^2$
n	iteration number
$\underline{n}$	unit surface normal vector
$\mathbf{q}$	flow state
$\underline{Q}(\underline{R},\underline{\rho})$	velocity kernel defined in Equation 4
R	rotor radius
$\underline{R}$	coordinate vector
S	surface
$\underline{S}$	vorticity source term
t	time
$\underline{u}$	velocity field
u_∞	free stream velocity field
V	volume
ν	viscosity
ρ	air density
ρ	source point coordinate vector
$\underline{\omega}$	vorticity vector
Ω	rotor rotation rate
Ω	coupling interface region

Presented at the American Helicopter Society Aeromechanics Specialists Meeting, San Francisco, CA, Jan. 20-22, 2010.

Introduction

Accurately and reliably determining the fluid dynamic environment is critical to the calculation of accurate rotorcraft performance. Since the helical wake usually remains near the rotor blades for an appreciable amount of time, inaccurate wake modeling leads to poor predictions of rotor blade loading, which in turn compromises predictions of the rotor wake. It is therefore apparent that correct prediction of the wake strength, structure and position is of critical importance, and both Lagrangian vortex methods and grid-based Computational Fluid Dynamics (CFD) techniques have been developed to numerically simulate rotor wake flows. However, while such analysis tools are capable of predicting the loading on rotors under various flight conditions, assumptions made during formulation and implementation constrain their application to general configurations.

A convenient way to simplify predicting rotary wing aerodynamics is to break it into two parts: analysis of the local aerodynamics (i.e. specifically the rotor blades,

but also the fuselage and other surfaces) and modeling of the flow in the environment surrounding the rotorcraft (i.e. the wake). Both the local and the global rotorcraft flow fields have been modeled, with varying degrees of success, using Lagrangian vortex methods and grid-based CFD, and the next few paragraphs serve to review commonly used techniques, and to highlight successes and potential shortcomings of these methods.

The aerodynamics of rotor blades has historically been modeled with vortex methods of varying sophistication. However these methods are limited in their ability to address viscous and compressible flow. While extensions of these methods can address compressibility and viscous effects to a limited degree, only Navier-Stokes CFD solvers are capable of reproducing all of the significant fluid dynamics mechanisms and producing good predictions of both steady and unsteady blade loading [1-3].

Lagrangian free-wake methods, where the rotor wake is modeled as a vortex filament (or a collection of vortex filaments) trailed from each blade, can predict sufficiently the wake induced loading on a rotor for a variety of flight conditions [4-11]. Such methods offer fast turnaround times, even real-time, and can be easily coupled to lifting-line and panel methods. While these approaches are ideally suited to propagating vortices over long distances and offer a compact flow description, their efficiency deteriorates for flight conditions where the rotor wake undergoes large scale distortions (e.g. strong wake on wake interactions such as vortex ring state, airframe interactions, and ground effect). In such situations, vortex methods become increasingly inaccurate and costly. Core distortions become pronounced and must be modeled empirically, and methods to account for compressibility and viscous effects are usually not included.

Traditional grid-based based CFD methods (i.e. velocity and pressure), do not make any a-priori assumptions about the shape and evolution of the flow-field. These techniques are, in principle, capable of modeling the formation, evolution, coalescence and rupture of the complete rotorcraft wake. Unfortunately, because of the helical/epicycloidal nature of the rotor wake, regions of strong vorticity remain near to the rotor for appreciable amounts of time, and the extended action of numerical diffusion, inherent in current differencing methods, upon these regions can quickly smear the vorticity leading to poor performance predictions.

The ability to preserve intense vortices and other localized flow features in rotorcraft flow-field calculations remains a major challenge to current numerical techniques, and many researchers have tried to solve the numerical diffusion-induced problem, with limited success, by increasing both the grid resolution and the accuracy of the numerical technique used to transfer flow properties from one grid cell to the next [12-19]. Vorticity Confinement [20-25] can also be added to the PV CFD formulation to ensure that angular momentum (i.e. circulation and thus vorticity) is conserved; however, spurious flow physics have been observed [22].

Attempts have also been made to combine the best features of CFD and vortex filament techniques [26-32] and whilst these coupled solutions generally yield improved performance predictions for a select number of flight conditions, they do, however, still suffer from numerical diffusion of the rotor wake, particularly near the blade tip, in the region where the wake has not rolled up sufficiently to start the Lagrangian solution [26, 33-35]. In addition, these techniques have difficulty modeling flight regimes where the rotor tip vortices pass close to the rotor blade [28, 36].

Lagrangian particle methods have also been coupled to CFD tools to address the diffusion of vorticity [37, 38], however, these methods typically suffer from the same limitations as their filament based counterparts, which is expected since vortex particles are functionally equivalent to short filament segments. Furthermore, while particle methods have been very successful at solving two-dimensional problems, difficulties associated with maintaining divergence-free vorticity fields and dealing with particle disorder [39], preclude routine application of such methods to high Reynolds number three-dimensional flows, such as those associated with rotorcraft.

Recently, it has been shown that numerical diffusion of the rotor wake can be controlled in a CFD solver – albeit, one based on a vorticity-velocity formulation – by carefully constructing the flux formula and selecting an appropriate flux limiter [40-42]. The Vorticity Transport Model (VTM), however, has not been developed to the extent where it can provide good a-priori predictions of blade aerodynamics, and is driven by a Weissinger-L panel method. This limitation motivated the development of a modular flow solver, VorTran-M, based on the CFD solver in VTM that can be coupled to a conventional Navier-Stokes code [43, 44]. In this arrangement, the Navier-Stokes solver is used to resolve the (presumably small) regions of compressible viscous flow near to the blades, and VorTran-M is applied to the remaining, vortex dominated flow domain. Such an arrangement simultaneously exploits the ability of traditional CFD to predict local aerodynamics and the low dissipation first principles wake modeling capabilities of VorTran-M in the wake.

Building upon the prior work presented in [43, 44], this paper reviews the development of VorTran-M, prior

coupling work and the general interfacing strategy. This paper concludes with a description of the integration of VorTran-M with the NASA CFD solver OVERFLOW [45] and presents preliminary results.

Hybrid Grid-Based CFD Solver Development

Overview of VorTran-M

VorTran-M solves the unsteady vorticity transport equation, which is obtained by taking the curl of the Navier-Stokes equations. Denoting the local flow velocity, $\underline{u}$, and the associated vorticity distribution, $\underline{\omega}=\nabla\times\underline{u}$, then for incompressible 3D flow this equation is stated as follows:

$$\frac{\partial}{\partial t}\underline{\omega}+\underline{u}\cdot\nabla\underline{\omega}-\underline{\omega}\cdot\nabla\underline{u}=\upsilon\nabla^2\underline{\omega}+\underline{S} \qquad (1)$$

where $\underline{S}$ is a vorticity source representing vorticity that arises on solid surfaces immersed in the flow. For rotary wing aircraft, the wake arises as a vorticity source associated with the aerodynamic loading of the rotor blades, fuselage, wings, and other parts of the vehicle. The velocity induced by this vorticity distribution at any point in space is governed by the Biot-Savart relationship,

$$\nabla^2\underline{u}=-\nabla\times\underline{\omega} \qquad (2)$$

which, when coupled to Equation 1, feeds back the strength and geometry of the rotor wake to the loading of the rotor blades and fuselage.

VorTran-M employs a direct numerical solution to Equations 1 and 2 to calculate the evolution of the rotor wake. At the beginning of each time step the numerical implementation calculates the velocity, $\underline{u}$, at which the vorticity field must be advected, by inverting Equation 2 with either cyclic reduction [40, 46, 47] or a Cartesian Fast Multipole method on an adaptive grid [41, 48, 49]. The vorticity distribution is then advanced through time using a discretized version of Equation 1, obtained using Toro's Weighted Average Flux (WAF) algorithm [50, 51] and Strang spatial splitting. This process is then repeated for each time step.

This numerical technique conserves vorticity explicitly, which has been shown to preserve the vortical structures of rotor wakes for very long times. Numerical diffusion still admits the spreading of vorticity, but this can be controlled by implementing a suitable flux limiter in the WAF scheme [52].

Figure 1, demonstrates the ability of this formulation to capture detail in the wake structure of a hovering rotor even with a relatively coarse grid (800,000 grid cells, 50 cells per rotor radius, 6 cells per blade chord) [44]. This example illustrates that if the vortical structures in the wake are accurately resolved, then the solution will show experimentally observed fluid dynamic phenomena such as the growth of the vortex pairing instability and the subsequent loss of symmetry in the wake downstream of the rotor.

Figure 1: Snapshot of vortex paring in the wake beneath a two bladed hovering rotor from [48]

Coupling the VorTran-M Module to Primitive Variable CFD

A general and versatile interfacing strategy for coupling traditional CFD methods to the VorTran-M module has been developed that inherently accounts for grid motion and supports multiple bodies in the flow through appropriately defined CFD/VorTran-M domains, time stepping strategies and techniques to transfer the flow states from one domain to another.

The coupling strategy is summarized in Figure 2. At each time step, vorticity (and/or velocity) is evaluated from the CFD solution and used to overwrite that in the VorTran-M module in a carefully specified overlap region (see Figure 3 and [44] for more details). This vorticity then evolves according to the vorticity transport equation. The influence of the wake upon the CFD solution is effected at the outer boundaries of the CFD domain where the velocities induced by the VorTran-M module are evaluated and used to set the outer boundary conditions. In this arrangement, the VorTran-M module is responsible for vorticity transport outside of the CFD domain, whereas the CFD solver handles the non-potential flow near the surfaces.

The procedure adopted for coupling the VorTran-M and CFD codes is motivated by several considerations regarding the underlying formulations and capabilities of the respective codes. To show why this approach was chosen over simpler or computationally less expensive alternatives, it is useful to review these considerations and explain how the present arrangement addresses them. To this end, the following constraints and properties for each software module are given.

1. In order to control numerical dissipation within the CFD solver at minimal cost, it is desirable to use a fine mesh over the smallest volume necessary. However, since the current VorTran-M is incompressible, the CFD grid must extend sufficiently far that the effects of compressibility outside the domain can be neglected (usually on the order of a chord length).
2. In a vorticity-velocity formulation, the velocity anywhere inside a domain is completely determined by the vorticity distribution over the domain and the velocity distribution over the domain boundary.
3. VorTran-M employs explicit time stepping.
4. In general, the CFD mesh will be moving relative to the one used by VorTran-M.
5. Vorticity (and/or velocity) is transferred from the CFD solution to the VorTran-M module where it is then evolved according to the vorticity transport equation. Steps must be taken to prevent "double counting" of vorticity by ensuring that once the vorticity is transferred to VorTran-M, it or its evolved derivative will not be projected again at a later time step.

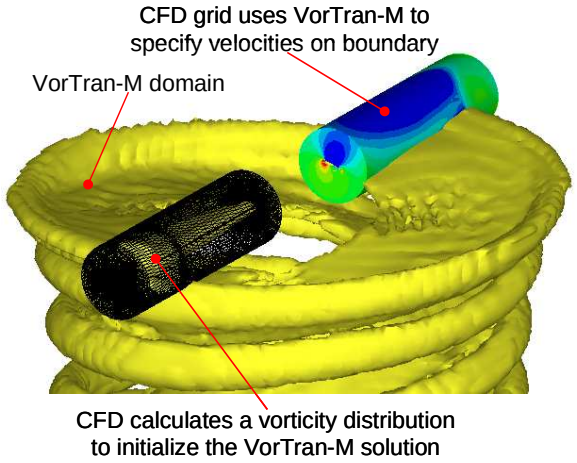

Figure 2: Schematic of multi-domain CFD/VorTran-M coupling

One way to address considerations 4 and 5 is to use an overwriting scheme where the VorTran-M vorticity in a selected region is overwritten with values from the CFD solution at every time step. This procedure, described in detail in [44] eliminates double counting and also facilitates the handling of moving grids, a requirement for efficient rotorcraft modeling. Overwriting is currently used in the VorTran-M module for transferring vorticity and/or velocity. While other options can be considered, the overwriting procedure appears to be the most effective in simultaneously accommodating general moving grids while retaining simplicity in both formulation and code implementation.

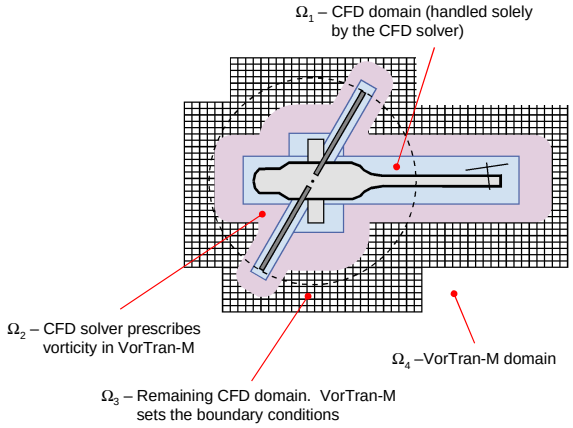

Figure 3: Detailed schematic of CFD/VorTran-M overlap regions

These considerations motivated the current approach that defines four regions in the flow domain and treats vorticity differently in each domain. These regions, summarized in see Figure 3, are defined as:

Ω_1: Lies inside CFD boundaries, and encloses all solid surfaces. The flow is represented entirely by the CFD solver. Ω_1, can be disjoint, as in Figure 2, but contains all solid bodies of interest.

Ω_2: Surrounds Ω_1 and lies inside CFD boundaries. The flow is represented by CFD solver. Vorticity and/or velocity is transferred to VorTran-M at the start of every time step, thus overwriting the VorTran-M solution in this region. VorTran-M evolves the vorticity during the time step to determine the amount of vorticity that advects out of Ω_2.

Ω_3: Consists of the remaining CFD domain lying outside of region Ω_2. Both VorTran-M and the CFD solver evolve the flow in the normal manner. This region is usually small, often only several cells thick, and facilitates solution stability by preventing instantaneous feedback between the solvers. The VorTran-M module sets the outer CFD boundary conditions. Selecting the best method for setting the outer CFD boundary conditions is an area of ongoing research.

Ω_4: Consists of the remaining VorTran-M domain lying outside of region Ω_3. The flow is entirely represented by VorTran-M.

Equivalent Vorticity and Velocity Distribution

It is well known that an unsteady, viscous and incompressible flow field in a bounded region can be

completely described in terms of its distributed vorticity and surface velocities [53, 54]. In the case of inviscid bounded flows, the finite surface velocities correspond to an infinitesimally thin shear layer whose vorticity must also be included in the representation. At high Reynolds numbers, the regions where vorticity is significant are usually compact, occupying small regions of space (wakes, the solid surfaces and shed vortices). Thus, a vorticity-based representation of the flow field is likely to require far less storage than one based upon primitive flow variables.

Given a vorticity distribution, $\underline{\omega}$, inside a flow volume, *V*, with bounding surface, S, the velocity field, $\underline{u}$, at any point, $\underline{R} \in V$, can be obtained from the generalized Biot-Savart relation [53, 54]:

$$\underline{u}(\underline{R}) = u_\infty + \int_V \underline{\omega}(\underline{\rho}) \times \underline{Q}(\underline{R}, \underline{\rho})\, dV + \oint_S [\underline{u}(\underline{\rho}) \cdot \underline{n} + (\underline{n} \times \underline{u}(\underline{\rho})) \times] \underline{Q}(\underline{R}, \underline{\rho})\, dS \quad (3)$$

where $\underline{n}$ is the unit surface normal vector pointing into the flow, and

$$\underline{Q}(\underline{R}, \underline{\rho}) = \frac{1}{4\pi} \frac{\underline{R} - \underline{\rho}}{\left| \underline{R} - \underline{\rho} \right|^3} \quad (4)$$

The surfaces can be chosen to lie a small distance away from the solid walls such that they encompass the significant non-potential flow features (shocks and boundary layers). The influence of the flow inside the enclosed surface upon the outer region is then completely accounted for in terms of the surface velocities. This is preferable to calculating the interior vorticity field and invoking the Biot-Savart law because the latter presumes simpler flow physics (e.g., incompressible flow for this form of Equation 3) than is actually present. Applying Equation 3 on the other hand remains completely general provided that the exterior region is governed by potential flow. It then provides a formally legitimate way of characterizing the influence of non-potential flow upon the remainder of the flow domain. It also avoids potential problems associated with the effective vorticity of solid bodies executing rigid body and deformational motions. Other than its inherent discrete approximations, Equation 3 provides a complete description of the flow field provided that the vorticity and the surface velocities are known.

Time Stepping Strategy

A time stepping strategy is defined that consists of advancing both the CFD and VorTran-M solutions forward in time and then overwriting the VorTran-M solution in Ω_2 using the CFD results.

At time t^n, a solution in both the CFD and VorTran-M domains is available. This solution is advanced to the next time level, t^{n+1}, using the respective integration strategies. In most arrangements, an implicit time marching strategy is used in the CFD code where the discrete set of equations defining the flow field update, $\mathbf{q}_{CFD}^{n+1} - \mathbf{q}_{CFD}^{n}$ are evaluated at t^{n+1}. Since VorTran-M employs an explicit scheme it is most convenient to first advance the VorTran-M solution to t^{n+1} so that the resulting flow field, $\underline{\omega}_{VorTran-M}^{n+1}$ and $\mathbf{q}_{VorTran-M}^{n+1}$, are available to evaluate flow states at the CFD boundary. Once both the VorTran-M and CFD solvers have advanced the solution to t^{n+1}, the overwrite step is performed where the CFD solution in Ω_2 (which may differ from step to step) overwrites the VorTran-M solution.

Prior CFD/VorTran-M Couplings

An important goal of prior work [44, 55] was to demonstrate the feasibility of successfully and efficiently implementing such a hybrid arrangement and identifying and addressing key numerical issues arising from the interface treatment. VorTran-M has been coupled to two different in-house CFD solvers, a deforming and moving unstructured grid RANS solver and a Cartesian grid solver.

Unstructured CFD/VorTran-M

CDI's Rotor Stator Analysis in 3D (RSA3D) was originally developed to model aeroelastic rotor-stator interaction problems, and can also analyze flows over propellers, rotors, complex multistage compressors/turbines and cascades [56-59]. RSA3D was developed under the sponsorship of NASA Glenn Research Center and was the subject of continued development and refinement from 1990-1998.

The flow analysis used in the RSA3D analysis solves the RANS equations on an unstructured deforming grid using multigrid acceleration strategies [56]. It also includes an efficient quad-tree-based interpolation scheme to handle the sliding rotor-stator interface in a consistent and conservative manner, as well as an optional containment-dual based discretization scheme to reduce dissipation on high aspect ratio grids [57-59].

RSA3D and VorTran-M were coupled together using a direct cell intersection method based on the coupling strategy described above [44]. Excellent results were obtained for the steady and unsteady lift response for an impulsively started wing and the unsteady loading on a wing at 90^o angle of attack [44]. Sample rotor wake predictions for an untrimmed two-bladed rotor are shown in Figure 4.

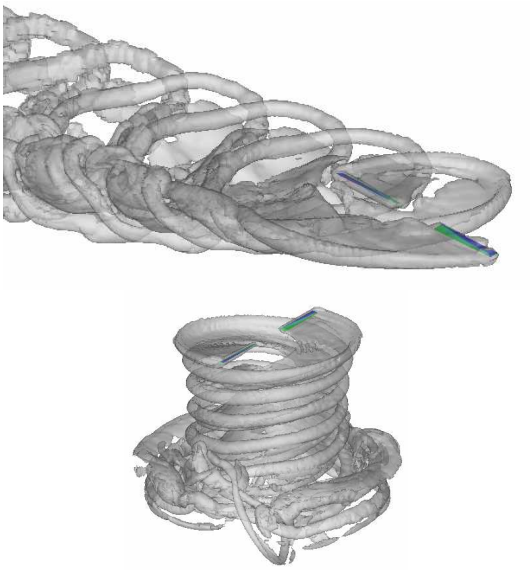

Figure 4: RSA3D/VorTran-M rotor wake predictions: two bladed untrimmed rotor in forward flight (upper) and two bladed untrimmed rotor in slow speed ascent (lower) from [44]

Cartesian Grid/VorTran-M

CDI's Cartesian Grid Euler (CGE) solver determines the unsteady flow field by solving the compressible (3D) Euler equations upon a Cartesian grid structure consisting of a hierarchical collection of nested cube-shaped cells (an octree). A central element in the Cartesian grid concept is reliance upon intersection methods to generate the cell volumes and areas at the surfaces rather than attempting to align the mesh with the complex surfaces. Once a surface geometry definition is provided, the subsequent grid generation and flow computation can proceed autonomously since the Cartesian mesh does not need to be boundary conforming. Moreover, while primarily intended to solve compressible flows, CGE has also been shown to behave well for low speed flows with Mach number less than 0.1.

Recently, CDI coupled CGE and VorTran-M for the development of the *first* commercial ship awake database for a real-time tactical flight simulator [55]. This effort, for the US Navy's MH-60R/SH-60B tactical operational flight trainers, included over 192 ship/flow condition combinations, with the wake flow field sampled at ≤1m spacing out to 4 ship lengths downstream of the ship. The coupled CGE/VorTran-M was selected for this effort since

1. Flow separation points, on bluff bodies with sharp edges (i.e. ships), do not need to be explicitly specified since the computational scheme ensures that Kutta conditions are implicitly enforced at sharp corners and edges. Thus, the critical flow features of the ship airwake, which are dominated by bluff body separation and vortex shedding, can be captured by an inviscid Euler formulation, and enormous reductions in CPU time can be gained over alternative viscous CFD approaches.
2. Viscous flow effects are significant only in localized regions near to the ship surface. Outside this boundary layer region, small-scale flow features, for which viscous solvers would be required, do not induce aerodynamic forces on the helicopter that are relevant to piloted flight simulations. The aerodynamic forces resulting from these small-scale flow features are effectively filtered by the flight dynamic response of the helicopter.
3. The requirement to resolve the vorticity in the ship airwake at ≤1m spacing at least 4 ship lengths downstream would need an intractably fine grid resolution using conventional CFD methods.

A sample ship airwake prediction is shown for a LPD-4 class ship in Figure 5.

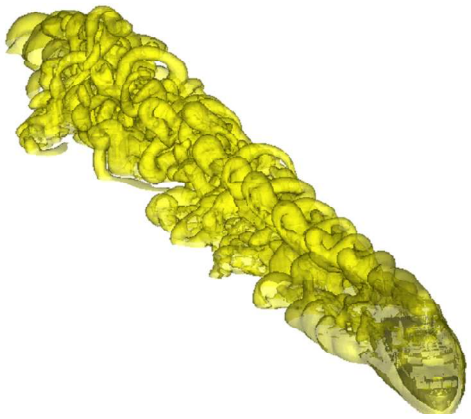

Figure 5: CGE/VorTran-M prediction of a LPD-4 class ship airwake

Coupling to OVERFLOW

Preliminary-Vorticity-Based Coupling

A preliminary vorticity-based coupling between OVERFLOW 2.1ab and VorTran-M was undertaken using the methodology described above. This approach, (see Figure 6) was minimally invasive to OVERFLOW, with minor modifications required to only five subroutines, and supports the fully parallel implementations. Moreover, since OVERFLOW automatically initiates VorTran-M this coupling procedure is general enough to support any configuration, future OVERFLOW code releases and multi-processor developments of VorTran-M.

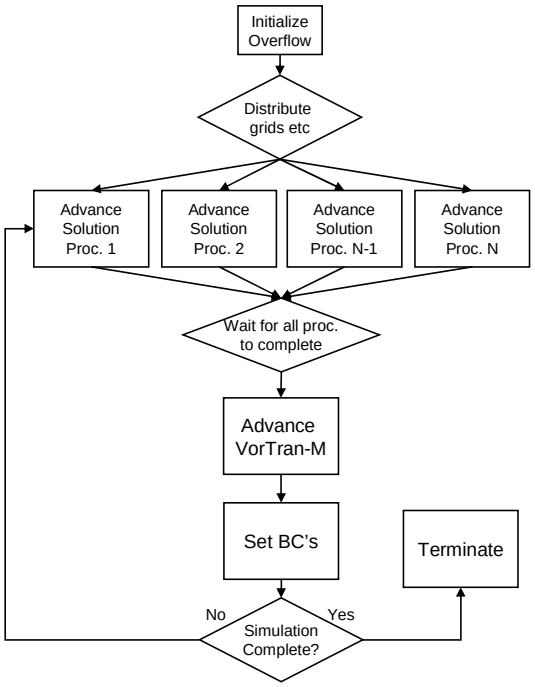

Figure 6: Overall OVERFLOW/VorTran-M coupling procedure

Predictions for a single-bladed rotor configuration (see Figure 7) in forward flight are presented in Figure 8 through Figure 10. The rotor configuration consisted of a modified NACA 0012 airfoil section (O-grid with 91 x 89 x 31 cells) and two end caps (67 x 39 x 41 cells each). A body of revolution representing a rotor hub (71 x 121 x 37 cells) was also included in the analysis. To facilitate the vorticity-based coupling a non rotating outer rectangular grid domain (271 x 271 x 52 cubic cells with $\Delta s \approx 0.22c$) contained the entire rotor system described here, and was used to calculate the vorticity required by VorTran-M. Pure OVERFLOW results are presented that utilized an off-body grid system where the grid levels coarsened by a factor of two between the near-field of the rotor system to the far field region of the computational domain. For the hybrid OVERFLOW/VorTran-M case where the OVERFLOW outer near body grid was used to input the vorticity for VorTran-M, the finest cell size in the VorTran-M domain was then set to twice the size of the near body grid ($\Delta s \approx 0.43c$) cell, and the subsequent grid coarsening occurred at every rotor radius downstream.

Results are presented in Figure 8 after 2550 time steps (~630 degrees) and the starting vortex has convected about a diameter downstream. Here, the extent of the OVERFLOW near body grids is outlined in red and the active VorTran-M grid in blue. On these grids, the pure OVERFLOW computation is normally dissipative in nature and hence unable to preserve significant vorticity in the rotor wake beyond one rotor revolution at most. The coupled OVERFLOW/VorTran-M solution, on the other hand, is able to preserve the entire wake flow, including the starting vortex, see Figure 8 right.

A direct comparison of the predicted vorticity field (non-dimensional OVERFLOW units scaled by the speed of sound) for these two solutions is shown on the slices, perpendicular to the direction of flight , downstream of the rotor plane, see Figure 9 and Figure 10.

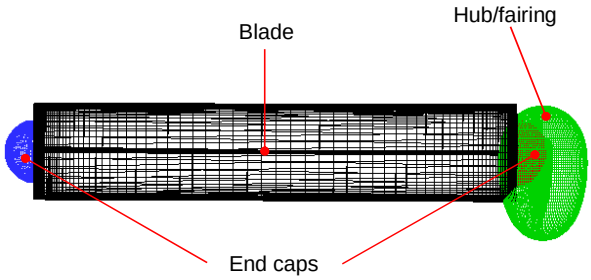

Figure 7: 1 bladed rotor and hub grid arrangement. Blade grid (black), root-cap (red) and body-of-revolution hub grid (green)

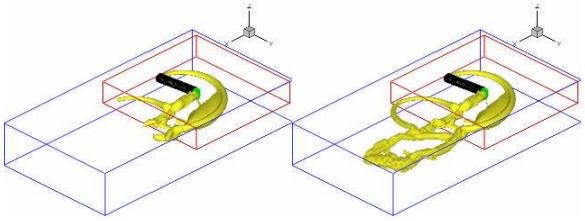

OVERFLOW *OVERFLOW/VorTran-M*

Figure 8: Predictions of wake vorticity, plotted at the same level of vorticity magnitude, for a 1-bladed rotor in forward flight after 2550 time steps

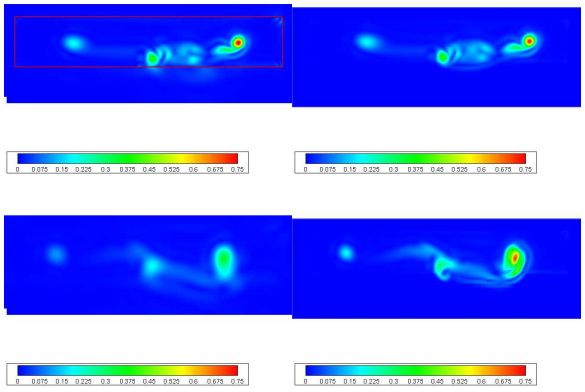

OVERFLOW *OVERFLOW/VorTran-M*

Figure 9: Predicted vorticity magnitude for a 1-bladed rotor in forward flight on a plane perpendicular to the direction of flight, 23.2 (upper) chord lengths and 31.7 (lower) downstream of the hub. $\Delta s_{OVERFLOW}$ (red region at left) ≈0.22c, $\Delta s_{OVERFLOW}$ ≈0.43c and $\Delta s_{VorTran\text{-}M}$≈0.43c

Figure 9 top compares the predictions on a slice 23.2 chord lengths aft of the rotor hub, and, despite the factor

of two cell size difference between the OVERFLOW near body grid (the red box in Figure 9 upper left) and VorTran-M, both show almost identical vorticity fields (peak vorticity for both cases is 0.77). Further downstream, 31.7 chords lengths (Figure 9 bottom), the solutions start to diverge with the OVERFLOW predicting a peak vorticity (0.36) that is half the OVERFLOW/VorTran-M value (0.72). By 33.3 chord lengths downstream (Figure 10 top), the VorTran-M grid for the hybrid calculation has been coarsened to twice the resolution of the corresponding OVERFLOW grid, yet the solution clearly demonstrates a high degree of the conservation of the peak vorticity. It is important to mention that the OVERFLOW solution has diffused the rotor blade tip vortex to a magnitude of 0.29 peak value, whereas the hybrid solver predicted a distinct core structure with peak of 0.79. Similar trends are shown at 40 chord lengths downstream in Figure 10 bottom, where the OVERFLOW predicted peak vorticity has been diffused to about 20% the value of the hybrid OVERFLOW/VorTran-M solution on a grid that is twice lower grid density.

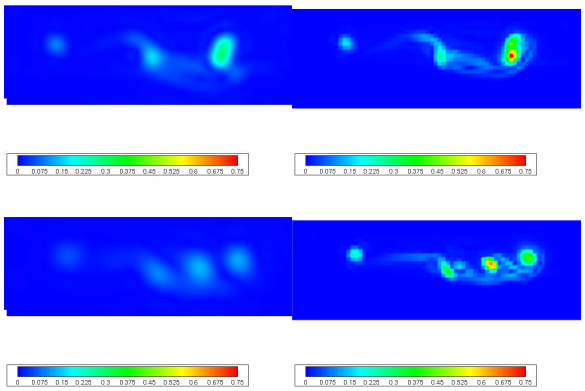

OVERFLOW *OVERFLOW/VorTran-M*

Figure 10: Predicted vorticity magnitude for a 1-bladed rotor in forward flight on a plane perpendicular to the direction of flight, 33 (upper) chord lengths and 40 (lower) downstream of the hub. $\Delta s_{OVERFLOW} \approx 0.43c$ *and* $\Delta s_{VorTran\text{-}M} \approx 0.87c$

Preliminary Velocity-Based Coupling

Whilst the preliminary OVERFLOW/VorTran-M coupling presented above produced promising results, a fine grid, surrounding all bodies in the flow, was required to accurately resolve the vorticity prior to transitioning to VorTran-M. The computational cost of this grid dominated the calculations. Implementing cell intersection routines, as in [44], would eliminate this grid requirement, however such methods are complicated, invasive and expensive.

In the late summer of 2009, a new, more general velocity-based coupling that builds upon the observations defining flows in terms of vorticity and velocity presented above and detailed in [44], was developed. Here, the velocity, rather than vorticity, is passed from OVERFLOW to VorTran-M at the VorTran-M cell corners in the overlap region. Within VorTran-M, the vorticity field is calculated by finite differencing the velocity field. This procedure is facilitated by setting up a near body grid in OVERFLOW that is identical to the finest VorTran-M grid. OVERFLOW treats this grid like any other, and automatically performs grid motion and hole cutting as the blades rotate, flap and, in the case of aeroelastic calculations, deform. The VorTran-M interface then uses this information to account for VorTran-M cells that have corners inside the body using a modified version of method described in [60]. At the end of each time step VorTran-M sets the OVERFLOW grid boundary conditions at the outer edge of this grid, or on any other grid in the solution.

Sample predictions for the 8^o collective, 1250 RPM Caradonna and Tung [61] hover experiments are presented below, where the two bladed zero twist rotor was meshed with three C-grids per blade (blade: 311 x 83 x 81 cells with y+=0.955, tip and root caps 85 x 79 x 61 cells) and the body of revolution hub from above. The two bladed rotor was then surrounded by the VorTran-M grid with 271 x 271 x 52 cubic cells ($\Delta s \approx 0.13c$). VorTran-M sets the boundary conditions on an additional grid of cubic cells with $\Delta s \approx 0.13c$ (112 x 58 x 36 cells that rotates with and encloses the rotor system, see Figure 11.

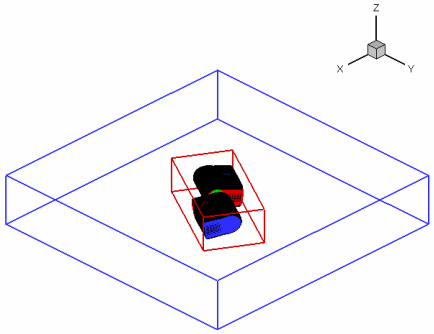

Figure 11: 2-bladed rotor and hub grid arrangement. Blade grids (black), tip-caps (blue), root-cap (red), hub grid (green), bounds of initial VorTran-M grid (blue line) and grid on which VorTran-M sets boundary conditions (red line)

The rotor wake after 5400 time steps predicted by the coupled OVERFLOW/VorTran-M is presented in Figure 12. The clean exiting and re-entering of the wake between the individual blade (OVERFLOW) and off body (VorTran-M) domains is clearly apparent, as is the starting vortex.

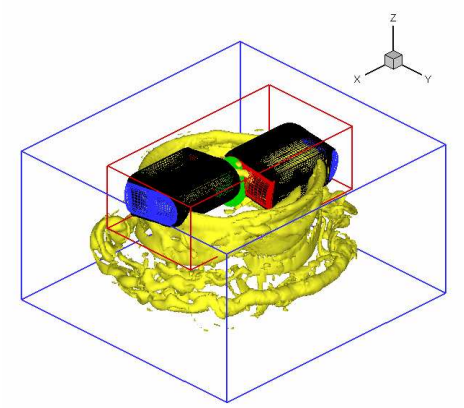

Figure 12: Iso-surface of vorticity magnitude illustrating the rotor wake predicted by OVERFLOW/VorTran-M after 5400 time steps

A close up of the rotor wake in the near-body region predicted with pure OVERFLOW and with the coupled OVERFLOW/VorTran-M is plotted in Figure 13, where OVERFLOW alone predicts very little root vorticity and significantly diffuses the tip vortices after about $\psi \sim 135^o$. Conversely, OVERFLOW/VorTran-M predicts significant loading along the entire span of the blade, with the tip vortices cleanly exiting the near-body region. The lack of inboard vorticity predicted by OVERFLOW also manifests in the rotor thrust coefficient and blade loading shown in Figure 14. OVERFLOW predicts the magnitude of the loading near to the tip, but significantly underpredicts the loading inboard of 0.8R. The integrated thrust coefficient for this case was C_T=0.00432, or 94% of the experimental value. OVERFLOW/VorTran-M more accurately reproduces the thrust coefficient (C_T=0.00458, or 99.6% of the experimental value) and the inboard loading. However, the 0.5R is still somewhat underpredicted, though this may be due to the relatively low number of revolutions simulated in these predictions. Nevertheless, the improved ability of OVERFLOW/VorTran-M to predict the spanwise loading for this hovering rotor configuration is significant.

Predictions of the tip vortex trajectory are compared to experimental measurements in Figure 15 where the error bars represent the error associated with locating the center of the tip vortex (i.e. local grid cell size). Given the early nature of the OVERFLOW/VorTran-M calculations and the complexity associated with the starting vortices and their interaction with the next revolution of wake (see Figure 12), tip vortex trajectories are only identified for the first 360° of wake age. Wake trajectory data was extracted from the pure OVERFLOW prediction for the first 270°, after which the predicted vorticity was insufficient to identify discrete vortices. Plotting Q-criterion may aid tip vortex identification, however all results presented here are based on iso-surface of vorticity magnitude.

Both solutions correctly predict the first 45° of tip vortex evolution; for the next 180°, however OVERFLOW predicts a tip vortex trajectory that is more outboard and lower than the measured data. Once significant wake interactions take place to distort the tip vortices (after 180° tip vortices start to interact with the next blade), OVERFLOW predicts a significant increase in both the descent and contraction rates. OVERFLOW/VorTran-M, correctly predicts the tip vortex trajectory for the entire revolution, with both the vertical and radial position of the wake correctly predicted throughout. OVERFLOW/VorTran-M also correctly predicts the asymptotic extent of radial contraction.

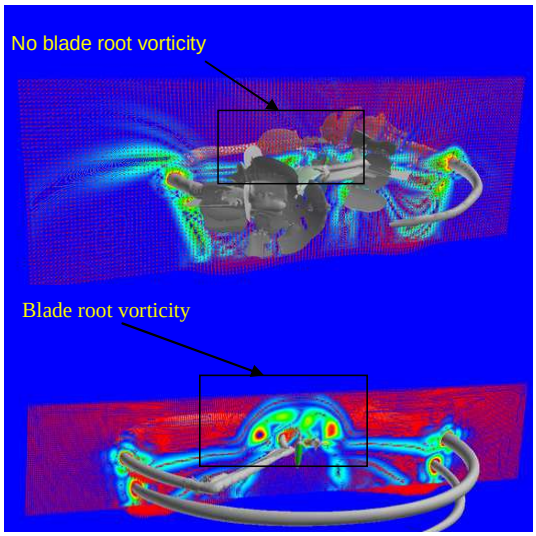

Figure 13: Close-up of OVERFLOW (upper) and OVERFLOW/VorTran-M (lower) predictions of the near-body wake and velocity vectors on a slice through the rotor

Figure 16 shows the time history for OVERFLOW and OVERFLOW/VorTran-M for the first 6000 iterations. The OVERFLOW time history shows strong low frequency unsteadiness in the integrated loads which persist across the entire solution (even out to 20,000 time steps); interestingly this large amplitude behavior is absent in the OVERFLOW/VorTran-M time history. One can therefore postulate that a "converged" quasi-periodic solution could be reached in fewer time steps with OVERFLOW/VorTran-M without the need to use special far field boundary conditions in conjunction with larger grid densities, as is the norm for hover predictions. However, caution should be taken to ensure that the starting vortices have convected far enough away from the rotor to ensure that their influence on the loading is minimal.

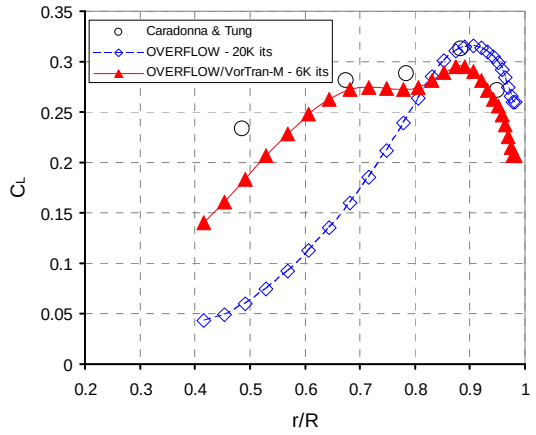

Figure 14: Comparison of measured and predicted spanwise loading ($C_{T\ Experiment}$ = 0.0046, $C_{T\ OVERFLOW}$ = 0.00432, $C_{T\ OVERFLOW/VorTran=M}$ = 0.00458)

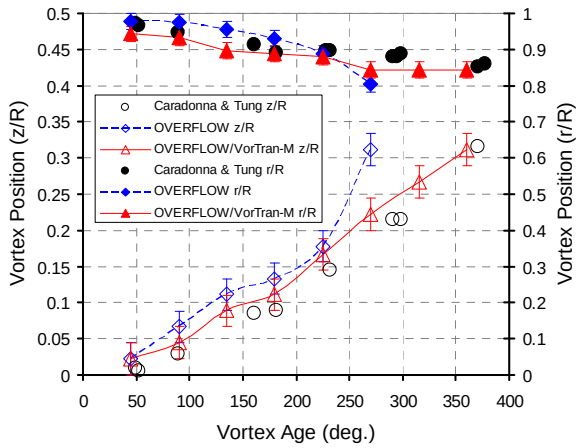

Figure 15: Comparison of measured and predicted tip vortex trajectory

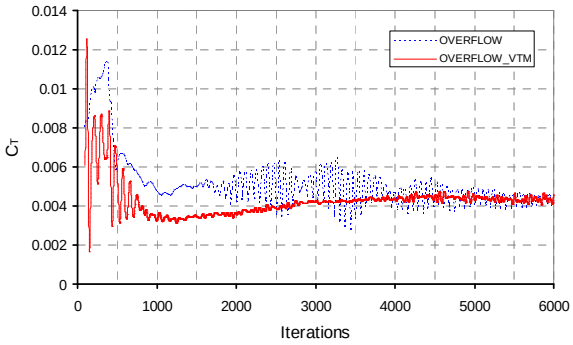

Figure 16: Convergence Time History

Conclusions

This paper describes the preliminary development of hybrid coupling between OVERFLOW and VorTran-M with the goal of improving predictions of rotorcraft flows by eliminating the vorticity diffusion issue that limits the application of pure RANS solvers. The coupling procedure has been described, along with several test cases. These preliminary results demonstrate improved wake prediction, along with spanwise loading for a hovering rotor.

Ongoing and Future Work

Work to date has focused on developing and demonstrating the feasibility a prototype hybrid OVERFLOW/VorTran-M CFD solver. Ongoing work seeks to improve the efficiency of the coupling in addition to further validation of the approach. It is anticipated that future work will investigate developing a parallel VorTran-M module, as well as refining the fundamental module coupling strategy to facilitate interfacing to a variety of CFD solvers.

Acknowledgements

The authors wish to acknowledge Dr Alexander Boschitsch of Continuum Dynamics, Inc. and Professor Richard Brown of the University of Glasgow, whose input and guidance were of great value during this effort. We would also like to acknowledge the support of the US Army Aero Flight Dynamics Directorate of Ames Research Center, specifically Mr. Mark Potsdam and Dr. Chee Tung, who guided the initial VorTran-M development and early OVERFLOW coupling work through the Small Business Innovative Research (SBIR) Program.

References

1. Dietz, W., L. Wang, Y. Wenren, F.X. Caradonna, and J. Steinhoff. "The Development of a CFD-Based Model of Dynamic Stall." American Helicopter Society 60th Annual Forum. 2004. Baltimore, MD.
2. Smith, M.J., T.-C. Wong, M. Potsdam, J. Baeder, and S. Phansee, "Evaluation of CFD to Determine Two-Dimensional Airfoil Characteristics for Rotorcraft Applications." Journal of the American Helicopter Society, 2006. **Vol. 51**(1): p. 70-79.
3. Smith, M.J., B. Koukol, T.R. Quackenbush, and D.A. Wachspress. "Reverse- and Cross-Flow Aerodynamics for High-Advance-Ratio Flight." 35th European Rotorcraft Forum. 2009. Hamburg, Germany.
4. Bagai, A. and J.G. Leishman, "Rotor Free-Wake Modeling Using a Relaxation Technique - Including Comparisons with Experimental Data." Journal of the American Helicopter Society, 1995. **40**(3): p. pp.29-41.
5. Bhagwat, M.J. and J.G. Leishman, "Rotor Aerodynamics During Maneuvering Flight Using a Time-Accurate Free-Vortex Wake." Journal of the American Helicopter Society, 2003. **48**(3): p. 143-158.

6. Johnson, W. "Technology Drivers in the Development of CAMRAD II." NASA/AHS Aeromechanics Specialists Conference. 1994. San Francisco.
7. Johnson, W. "Rotorcraft Aerodynamics Models for Comprehensive Analysis." 54th Annual Forum of the American Helicopter Society. 1998. Washington, D.C.
8. Quackenbush, T.R. and D.B. Bliss, "Free Wake Flow Field Calculations for Rotorcraft Interactional Dynamics." Vertica, 1990. **14**(3): p. 313-327.
9. Quackenbush, T.R., D.B. Bliss, and D.A. Wachspress, "New Free-Wake Analysis of Rotorcraft Hover Performance Using Influence Coefficients." Journal of Aircraft, 1989. **26**(12): p. pp.1090-1097.
10. Wachspress, D.A., T.R. Quackenbush, and A.H. Boschitsch. "First-Principles, Free-Vortex Wake Model for Helicopters and Tiltrotors." 59th Annual Forum of the American Helicopter Society. 2003. Phoenix, AZ.
11. Wachspress, D.A., T.R. Quackenbush, and A.H. Boschitsch, "Rotorcraft Interactional Aerodynamics with Fast Vortex/Fast Panel Methods." Journal of the American Helicopter Society, 2003. **Vol. 48**(No. 4).
12. Usta, E., "Application of a Symmetric Total Variation Diminishing Scheme to Aerodynamics of Rotors." 2002, Georgia Institute of Technology.
13. Usta, E. and L.N. Sankar. "Application of High Order Schemes to Aerodynamics of Hovering Rotors." AHS Aerodynamics, Acoustics, and Test and Evaluation Technical Specialists Meeting. 2002. San Francisco, CA.
14. Usta, E., B.E. Wake, T.A. Egolf, and L.N. Sankar. "Application of Symmetric Total Variation Diminishing Scheme to Aerodynamics and Aeroacoustics of Rotors." 57th Annual Forum of the American Helicopter Society. 2001. Washington, D.C.
15. Kim, H., M.H. Williams, and A.S. Lyrintzis, "Improved Method for Rotor Wake Capturing." Journal of Aircraft, 2002. **Vol.39**(No. 5): p. pp. 794-803.
16. van der Ven, H. and O.J. Boelens. "Towards Affordable CFD Simulations of Rotors in Forward Flight - A Feasibility Study with Future Applications to Vibrational Analysis." American Helicopter Society 59th Annual Forum. 2003. Phoenix, AZ.
17. Duque, E.P.N., L.N. Sankar, S. Menon, O. Bachau, S. Ruffin, M. Smith, K. Ahuja, K.S. Brentner, L.N. Long, P.J. Morris, and F. Gandhi. "Revolutionary Physics-Based Design Tools for Quiet Helicopters." 44th AIAA Aerospace Sciences Meeting and Exhibit. 2006. Reno, NV: AIAA-2006-1068.
18. Potsdam, M.A. and R.C. Strawn, "CFD Simulations of Tiltrotor Configurations in Hover." Journal of the American Helicopter Society, 2005. **Vol. 50**(No. 1): p. pp. 82-94.
19. Strawn, R.C. and M.J. Djomenhri, "Computational Modeling of Hovering Rotor and Wake Aerodynamics." Journal of Aircraft, 2002. **Vol. 39**(No. 5): p. pp. 786-793.
20. Costes, M. "Analysis of the VC2 Vorticity Confinement Scheme." 62nd Annual Forum of the American Helicopter Society. 2006. Phoenix, AZ.
21. Dietz, W., M. Fan, J. Steinhoff, and Y. Wenren. "Application of Vorticity Confinement to Prediction of the Flow over Complex Bodies: A Survey of Recent Results." AIAA CFD Conference. 2001. Anaheim, CA.
22. Steinhoff, J., Y. Wenren, and F.X. Caradonna. "Application of Vorticity Confinement to Rotorcraft Flows." 31st European Rotorcraft Forum. 2005. Firenze, Italy.
23. Wang, C.M., J.O. Bridgeman, J.S. Steinhoff, and W. Yonghu. "The Application of Computational Vorticity Confinement to Helicopter Rotor and Body Flows." 49th Annual Forum of the American Helicopter Society. 1993. St. Louis, Missouri.
24. Wenren, Y., M. Fan, W. Dietz, G. Hu, C. Braun, J. Steinhoff, and B. Grossman. "Efficient Eulerian Computation of Realistic Rotorcraft Flows Using Vorticity Confinement." 39th AIAA Aerospace Sciences Meeting and Exhibit. 2001. Reno, NV.
25. Wenren, Y., M. Fan, L. Wang, M. Xiao, and J. Steinhoff, "Application of Vorticity Confinement to Prediction of the Flow over Complex Bodies." AIAA Journal, 2003. **Vol. 41**(5): p. 809-816.
26. Bhagwat, M.J., M.A. Moulton, and F.X. Caradonna. "Development of a CFD-Based Hover Performance Prediction Tool for Engineering Analysis." American Helicopter Society 61st Annual Forum. 2005. Grapevine, TX.
27. Hariharan, N. and L.N. Sankar. "A Review of Computational Techniques for Rotor Wake Modeling." 38th Aerospace Sciences Meeting & Exhibit. 2000. Reno, Nevada.
28. Khanna, H. and J.D. Baeder. "Coupled Free-Wake/CFD Solutions for Rotors in Hover Using a Field Velocity Approach." 52nd Annual Forum of the American Helicopter Society. 1996. Washington, D.C.
29. Moulton, M.A., J.O. Bridgeman, and F.X. Caradonna. "Development of an Overset/Hybrid CFD Method for the Prediction of Hovering Performance." 53 Annual Forum of the American Helicopter Society. 1997. Virginia Beach, VA.

30. Moulton, M.A., Y. Wenren, and F.X. Caradonna. "Free-Wake Hover Flow Prediction with a Hybrid Potential/Navier-Stokes Solver." AHS 55th Annual Forum. 1999. Montreal, Canada: American Helicopter Society.
31. Roberts, T.W. and E.M. Murman. "A Computational Method for Helicopter Vortex Wakes." AIAA 17th Fluid Dynamics, Plasma Dynamics, & Lasers Conf. 1984. Snowmass, CO.
32. Roberts, T.W. and E.M. Murman. "Solution Method for a Hovering Helicopter Rotor Using the Euler Equations." AIAA 23rd Aerospace Sciences Meeting. 1985. Reno, NV.
33. Bhagwat, M.J., M. Moulton, and F.X. Caradonna. "Recent Advances in the Embedded-Wake Approach to Hover Performance Prediction." AHS 4th Decennial Specialist's Conference on Aeromechanics. 2004. San Francisco, CA.
34. Datta, A., J. Sitaraman, J.D. Baeder, and I. Chopra. "Analysis Refinements for Prediction of Rotor Vibratory Loads in High-Speed Forward Flight." American Helicopter Society 60th Annual Forum. 2004. Baltimore, MD.
35. Datta, A., J. Sitaraman, I. Chopra, and J.D. Baeder. "Improved Comprehensive Analysis for Prediction of Rotor Vibratory Loads in High-Speed Forward Flight." American Helicopter Society 60th Annual Forum. 2004. Baltimore, MD.
36. Berkman, M.E., L.N. Sankar, C.R. Berezin, and M.S. Torok. "A Navier-Stokes/Full Potential/Free Wake Method for Advancing Multi-Bladed Rotors." 53rd American Helicopter Society Annual Forum. 1997. Virginia Beach, VA.
37. Anusonti-Inthra, P. "Development of Rotorcraft Wake Capturing Methodology Using Fully Coupled CFD and Particle Vortex Transport Method." 62nd Annual Forum of the American Helicopter Society. 2006. Phoenix, AZ.
38. Zhao, J. and C. He. "A Viscous Vortex Particle Model for Rotor Wake and Interference Analysis." 64th Annual Forum of the American Helicopter Society. 2008. Montreal, Canada.
39. Cottet, G.-H. and P.D. Koumoutsakos, Vortex Methods: Theory and Practice. 2000, Cambridge, UK: Cambridge University Press. pp.313.
40. Brown, R.E., "Rotor Wake Modeling for Flight Dynamic Simulation of Helicopters." AIAA Journal, 2000. **Vol. 38**(No. 1): p. 57-63.
41. Brown, R.E. and A.J. Line, "Efficient High-Resolution Wake Modeling Using the Vorticity Transport Equation." AIAA Journal, 2005. **Vol. 43**(No. 7): p. 1434-1443.
42. Brown, R.E. and G.R. Whitehouse, "Modelling Rotor Wakes in Ground Effect." Journal of the American Helicopter Society, 2004. **Vol. 49**(No. 3): p. 238-249.
43. Whitehouse, G.R., A.H. Boschitsch, T.R. Quackenbush, D.A. Wachspress, and R.E. Brown. "Novel Eulerian Vorticity Transport Wake Module for Rotorcraft Flow Analysis." 8th Symposium on Overset Composite Grids & Solution Technology. 2006. Houston, TX.
44. Whitehouse, G.R., A.H. Boschitsch, T.R. Quackenbush, D.A. Wachspress, and R.E. Brown. "Novel Eulerian Vorticity Transport Wake Module for Rotorcraft Flow Analysis." 63rd Annual Forum of the American Helicopter Society. 2007. Virginia Beach, VA.
45. Slotnick, J.P., P.G. Buning, and R.H. Nichols. "OVERFLOW Flow Solver Overview." 8th Symposium on Overset Composite Grids & Solution Technology. 2006. Houston, TX.
46. Schumann, U. and R.A. Sweet, "A Direct Method for the Solution of Poisson's Equation with Neumann Boundary Conditions on a Staggered Grid of Arbitrary Size." Journal of Computational Physics, 1976. **Vol. 20**(No. 2): p. pp. 171-182.
47. Whitehouse, G.R. and R.E. Brown, "Modelling the Mutual Distortions of Interacting Helicopter and Aircraft Wakes." Journal of Aircraft, 2003. **Vol. 40**(No. 3): p. pp. 440-449.
48. Line, A.J., "Computational Modelling of Helicopter High-Frequency Dynamics." 2005, PhD Thesis, Department of Aeronautics Imperial College London.
49. Line, A.J. and R.E. Brown. "Efficient High-Resolution Wake Modelling using the Vorticity Transport Equation." 60th Annual Forum of the American Helicopter Society. 2004. Baltimore, MD.
50. Toro, E.F. "A Weighted Average Flux Method for Hyperbolic Conservation Laws." Royal Society of London, Series A: Mathematical and Physical Sciences,. 1989.
51. Toro, E.F., Riemann Solvers and Numerical Methods for Fluid Dynamics: A Practical Introduction. 2nd ed. ed. 1999, Berlin: Springer-Verlag.
52. Brown, R.E., "Rotor Wake Modeling for Flight Dynamic Simulation of Helicopters." AIAA Journal, 2000. **Vol. 38**(1): p. 57-63.
53. Wu, J.C., "Theory for Aerodynamic Force and Moment in Viscous Flows." AIAA Journal, 1981. **Vol. 19**(No. 4): p. pp. 432-441.
54. Wu, J.C. and N.L. Sankar. "Aerodynamic Force and Moment in Steady and Time-Dependent Viscous Flows." 18th Aerospace Sciences Meeting. 1980. Pasadena, CA.: AIAA-80-0011.
55. Keller, J.D., G.R. Whitehouse, A.H. Boschitsch, J. Nadal, J. Jeffords, and M. Quire. "Computational Fluid Dynamics for Flight Simulator Ship Airwake Modeling." Interservice/Industry Training,

Simulation, and Education Conference (I/ITSEC) 2007. 2007. Orlando, FL.
56. Boschitsch, A.H. and T.R. Quackenbush. "Adaptive Grid Computation of Transonic Flows Through Cascades and Investigation of Chordwise Bending Upon Aeroelastic Response." 32nd AIAA Aerospace Sciences Meeting & Exhibit. 1994. Reno, NV.: AIAA-1994-0145.
57. Boschitsch, A.H. and T.R. Quackenbush, "High Accuracy Fluid-Structure Interaction in Transonic Cascades," 31st AIAA Aerospace Sciences Meeting. 1993, AIAA-1993-0485: Reno, NV.
58. Boschitsch, A.H. and T.R. Quackenbush. "Prediction of Rotor Aeroelastic Response Using a New Coupling Scheme." Fifth Workshop on Dynamics and Aeroelastic Stability Modeling of Rotorcraft Systems. 1993. Rensellaer Polytechnic Institute, Troy, NY.
59. Boschitsch, A.H. and T.R. Quackenbush. "Prediction of Rotor Aeroelastic Response Using a New Coupling Scheme." 25th AIAA Fluid Dynamics Conference. 1994. Colorado Springs, CO.: AIAA-1994-2269.
60. Kempka, S.N., J.H. Strickland, M.W. Glass, J.S. Peery, and M.S. Ingber, "Velocity Boundary Conditions for Vorticity Formulations of the Incompressible Navier-Stokes Equations." 1995, Sandia National Laboratories, SAND94-1735: Albuquerque, NM.
61. Caradonna, F.X. and C. Tung, "Experimental and Analytical Studies of a Model Helicopter Rotor in Hover." 1981, NASA-TM-81232, USAAVRADCOM TR-81-A-23.